Closed-loop particle motion control using laser-induced thermocapillary convective flows at the fluid/gas interface at micrometric scale

Ronald Terrazas Mallea[1,2], Aude Bolopion[2], Jean-Charles Beugnot[2], Pierre Lambert[1], Michael Gauthier[2]

***Abstract*—Non-contact actuation has gained a large interest over the last few years, and many works have been performed on magnetic actuation, dielectrophoresis or optical tweezers. Thermocapillary convective flows are an attractive alternative to manipulate micrometric scale particles at the water/air interface. These flows are generated when a surface tension stress is generated at the fluid/gas interface due to a thermal gradient. Laser heating allows to generate fast, localized flows that improve the actuation performance. In this paper, a closed-loop controller is used to control the particle motion. To design this controller, a model for the system is proposed and experimentally identified. Proof of concept experiments are performed using a 500-µm-diameter steel spherical particle that show that the particle can be successfully displaced towards a target position. The experimental results show that maximal particle velocities between 4-9 mm/s can be attained during the control phase which can be compared against some of the fastest actuation principles that use Marangoni effect.**

I. Introduction

Non-contact actuation has proved to be a promising solution to move micrometer scale objects. Several physical principles can be used to induce the movement of particles. Magnetic actuation is highly appreciated for the high forces that can be applied to the objects [1], [2]. Both open-loop and closed-loop control have been performed to control the displacements of magnetic particles on planes [3] or in the space [4–6]. Control strategies are also proposed to control independently several magnetic objects using the same external field [7], or to control embedded degrees of freedom such as the opening of a gripper [8]. Electrophoresis (which uses DC currents) can be used to manipulate particles as shown in [9] [10]. Dielectrophoretic effects (which use AC currents) are also commonly used as an actuation principle at micrometric scale. Many lab on chips dedicated to cell analysis include open-loop dielectrophoretic actuation [11], [12]. A few works deal with closed-loop control in 2D [13] [14]. Optical tweezers use the pressure radiation of the light to move objects. The particularity of this actuation principle is that the force applied by the laser is short range. Several objects can be controlled by switching the laser from one object to another at high speed [15], or by using holographic patterns of light to produce several independent traps [16, 17].

Manipulation via actuated flows is an alternative approach, which uses the flow motion to move the object. Different mechanisms can be used to onset the flow motion like: electroosmosis, electrohydrodynamics, micromechanical, thermocapillary pumping [18], among others. These mechanisms have been used to manipulate particles at the microscale [19], yeast cells [20], among other examples.

In this work, it is proposed to use thermocapillary convection, which is generated by Marangoni effect, as the actuation mechanism to generate flow motion. This principle has already been used in different manners to control the movement of particles. In [21, 22], the thermocapillary convective flow is generated by heating the bottom of a bubble interface using a light pattern inside a closed chamber filled with a fluid. The generated flow pushes the particle away if it is floating or pulls it towards the bubble microrobot if the particle is sunken. The bubble microrobot follows the light pattern (heat source), so the position of the bubble can be changed by displacing the light. The light patterns are either programmed by the [21] or controlled by human users using keyboard inputs [22]. Multiple microrobots can be controlled at the same time, opening the possibility to perform manipulation in parallel of multiple particles [21], [22].

A slightly different method was proposed in [23] and [24], where the thermocapillary convective flow is generated around bubble microrobots which are created by heating a laser-light absorbent substrate. In [24], manipulation in parallel of multiple 20-µm-diameter polystyrene beads is performed using a scanning mirror. The control is performed using an interface that enables a human user to create bubble microrobots and control their position in the liquid medium using a touch screen. In [25] a space light modulator is used to generate a laser pattern defining an array of laser spots which is then projected into the substrate. A sequence of patterns can be programmed in order to control the position of multiple bubble microrobots in parallel and independently. However, the control of the bubble microrobots remained manual, as the user had to define the position of each microrobot frame by frame.

In [26], Marangoni convective flow (which is also a consequence of the Marangoni effect) is generated by heating a water layer by the bottom using a laser. The generated flow is used to displace particles which are inside the fluid bulk.

From the state of the art, it can be seen that the Marangoni and thermocapillary convective flows are very promising actuation methods for particle manipulation even without the use of automatic controllers. The implementation of a closed-loop controller would improve the performance of these techniques. In our previous works [27] and [28], it was demonstrated that thermocapillary convective flows could be used to move

[1] Bio-, Electro- And Mechanical Systems department (BEAMS), Ecole Polytechnique de Bruxelles, Universite Libre de Bruxelles, 1050 Bruxelles, Belgium. rterraza@ulb.ac.be

[2] FEMTO-ST Institute, AS2M and Optics departments, Univ. Bourgogne Franche-Comté, Univ. de Franche-Comté/CNRS/ENSMM, 24 rue Savary, F-25000 Besançon, France aude.bolopion@femto-st.fr

micrometric size particles placed at the water/air interface with good performances in terms of the particle velocity. However, these experiments were performed without any type of controller so it was not possible to control the particle motion. The goal of this paper is to demonstrate that a closed-loop controller can allow to displace the particle towards a target position precisely. To design this controller, a model of the system is proposed and experimentally identified. With this controller, proof of concept experiments are performed on which a 500-µm-diameter steel sphere is displaced towards a desired target position with maximal attained velocities between 4-9 mm/s.

This paper is organized as follows. In section II, the experimental setup is described. In section III, the actuation principle is presented, modeled and experimentally identified. In section IV, a closed-loop controller for the system is defined. In section V, the experimental results are presented and analyzed. Finally, the conclusions are presented in section VI.

II. General Principle

A. Experimental Setup

Micrometric particles placed at the air/liquid interface can be displaced using actuated flows. One way to generate such flows is to modify the surface tension of the interface using heat, as explained in details in [27]. In this work, thermocapillary convective flow is generated using the experimental setup shown in figure 1. A detailed description is provided in [27]. Here, only the main components are presented. Two lasers are used in the setup which are coupled using a laser fiber coupler (Thorlabs WD202C-APC) into a single beam. Each laser has a specific function. The first one is a continuous-wave 1455 nm infrared laser (Keopsys Fiber Raman Laser) which wavelength is absorbed by the water so it is used to heat the water. As the infrared laser cannot be detected by the camera, a second continuous-wave 655 nm red laser is used to make the resulting coupled beam visible. The coupled beam is collimated using a 10x Olympus objective RMS10X. The collimated laser beam is directed towards a plastic container filled with distilled water, using a 2-DOF piezo-actuated tip/tilt mirror (Physik Instrumente S.334-2SL) which has a mechanical tip/tilt range of $\pm$ 25 mrad on each axis (equivalent to $\pm$ 50 mrad optical beam deflection). The laser position at the water surface can be controlled by changing the mirror tip/tilt angles. The mirror is connected to the PI Controller E-616.SS0x, which allows to linearly control the mirror deviation with an input voltage between 0-10 V. The measured *infrared* laser beam power reaching the water surface is 38 mW and the laser spot radius is around 0.625 mm. This laser power is absorbed by the water, heating the water surface and generating thermocapillary convective flow that is used to drive the particle movement.

The experiments are performed using stainless steel AISI 304 spherical particles with a diameter of 500 µm (Redhill Precision), which are deposed at the water surface. Due to the wetting phenomena, the particle can float, attaining a certain equilibrium position (a detailed analysis is performed in [29]). The water layer thickness is around 7.5 mm contained on a square plastic container with dimensions of 115 × 115 mm^2. The container is covered using a plastic lid in order to reduce the surface contamination through time. The container is on top of a PHLOX white led back light, which provides a uniform background illumination that facilitates the image recognition. The particle position is tracked using with a Photonfocus camera (MV-D1024-TrackCam) with a resolution of 1024×1024 pixels at a frame rate of 30 FPS. The camera is tilted 3.5° in order to have vision of the whole working space. In order to reduce the infrared light reflection coming to the camera sensor, an absorptive neutral density filter (Thorlabs NENIR40BC) is placed on top of it. For the camera optics, a 50 mm focal length lens is used together with a 10 mm extensor ring. The field of view is adjusted to be 65×65 mm^2 (one pixel represents 63.5 µm).

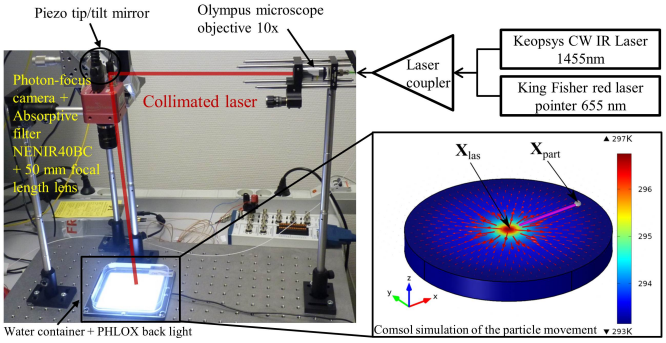

Fig. 1. Experimental setup for non-contact actuation using thermocapillary convective flows. A laser is pointed at position $\mathbf{X}_{\text{las}}$ in the water container, heating the region around it and defining a temperature field (represented by the color scale in the COMSOL simulation). The generated temperature gradient generates a surface tension stress at the interface that onsets the fluid flow (represented by the red arrows). The generated flow pushes a particle (gray sphere) whose position is given by $\mathbf{X}_{\text{part}}$, lying at the water/air interface. The particle moves in the direction of the flow which pushes it (the trajectory is represented by the magenta line). The COMSOL simulation shows the particle displacement after 2 seconds.

For control purposes, the experimental setup is considered as two subsystems: the Controlled mirror system and the Thermocapillary system (fig. 2). The "Controlled mirror system" block defines an open-loop controlled system that consists in the physical mirror ("Mirror" block) and an Inverse Mirror model that relates the desired laser position $\mathbf{X}_{\text{lasD}}$ to the real laser position $\mathbf{X}_{\text{las}}$. This block will be discussed in section II-B. The "Thermocapillary system" block includes the entire physical phenomena. It has as input the laser position $\mathbf{X}_{\text{las}}$ and as output the velocity of the particle $\dot{\mathbf{X}}_{\text{part}}$. This is the main block to identify in order to perform the control of the system. This block will be discussed in detail in section III.

B. Controlled mirror system

The "Mirror" block (Fig. 2) represents the piezo tip/tilt mirror that is used to control the laser beam position at the water surface $\mathbf{X}_{\text{las}}$ by changing the mirror tip/tilt angles. These angles are controlled using a voltage signal consisting of 2 channels $\mathbf{U}_{\text{mirr}} = (U_{\text{mirr}\,1}, U_{\text{mirr}\,2})$. These signals allow to point the laser beam over a surface defined as a rhombus with diagonals of lengths 36.9 mm and 56.2 mm in the x and y directions.

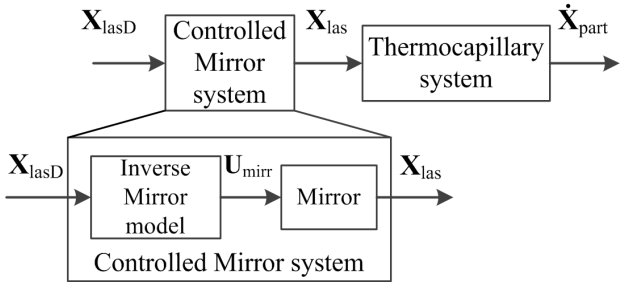

Fig. 2. Block representation. The Controlled mirror system includes the physical mirror and an Inverse Mirror model. The Thermocapillary system includes all the physics behind the particle movement.

The Inverse Mirror model defines the equations to compute a suitable voltage input signal $\mathbf{U}_{\text{mirr}}$ to obtain a desired laser position $\mathbf{X}_{\text{lasD}}$. This model is identified experimentally based on the mirror response. Various input voltages $\mathbf{U}_{\text{mirr}}$ by increments of 0.5 V are set, and the resulting laser positions $\mathbf{X}_{\text{las}}$ are measured using visual feedback. With this data, a second order polynomial relation is used to define $\mathbf{U}_{\text{mirr}}$ in function of the desired laser position $\mathbf{X}_{\text{lasD}}$, given by:

$$U_{\text{mirr}\,1} = a_{00} + a_{10}\, x_{\text{lasD}} + a_{01}\, y_{\text{lasD}} + a_{20}\, x_{\text{lasD}}^2 + a_{11}\, x_{\text{lasD}}\, y_{\text{lasD}} + a_{02}\, y_{\text{lasD}}^2 \quad (1a)$$

$$U_{\text{mirr}\,2} = b_{00} + b_{10}\, x_{\text{lasD}} + b_{01}\, y_{\text{lasD}} + b_{20}\, x_{\text{lasD}}^2 + b_{11}\, x_{\text{lasD}}\, y_{\text{lasD}} + b_{02}\, y_{\text{lasD}}^2 \quad (1b)$$

where $U_{\text{mirr}\,1}$, $U_{\text{mirr}\,2}$ are expressed in [V]. x_{lasD} and y_{lasD} are the cartesian components of $\mathbf{X}_{\text{lasD}}$ expressed in [mm]. The identified coefficients values are shown in table I.

TABLE I
MIRROR MODEL IDENTIFIED COEFFICIENTS

a_{00} [V]	3.204	b_{00} [V]	19.72
a_{10} [V/mm]	0.246	b_{10} [V/mm]	-0.277
a_{01} [V/mm]	-0.186	b_{01} [V/mm]	-0.187
a_{20} [V/mm^2]	2.80×10^{-4}	b_{20} [V/mm^2]	4.33×10^{-4}
a_{11} [V/mm^2]	3.83×10^{-4}	b_{11} [V/mm^2]	-4.44×10^{-4}
a_{02} [V/mm^2]	-9.89×10^{-5}	b_{02} [V/mm^2]	8.70×10^{-5}

In order to validate the model, a given set of 385 desired laser positions $\mathbf{X}_{\text{lasD}}$ are taken as reference data. For each one of those positions, the model is used to compute the corresponding set of voltages $\mathbf{U}_{\text{mirr}}$ which are then commanded to the mirror. The resulting position of each laser spot center $\mathbf{X}_{\text{las}}$ is measured experimentally. The maximal errors between the desired positions $\mathbf{X}_{\text{lasD}}$ and the obtained ones $\mathbf{X}_{\text{las}}$ are less than 41.3 µm in the x-direction and 86.9 µm in the y-direction. Compared to the the workspace size, these errors represent a deviation less than 0.11% and 0.15%, respectively. The resulting standard deviations in the x and y directions are 15 µm and 38 µm respectively.

The mirror has a response time of 10 ms where the thermocapillary system has an estimated response time of 800 ms (section III-D) and the camera provides a sampling time of 33 ms (30 FPS). So, the time delay of the mirror is considered negligible and the transfer function of the "Controlled Mirror system" block is considered to be equal to identity. If a faster camera would be used, the mirror response time may lead to some instabilities and it should be analyzed more carefully as mentioned in [30], [31].

III. THERMOCAPILLARY SYSTEM

The goal of this section is to identify the relation between the laser position and the resulting particle movement. The physical principle is detailed and used to get a model of the Thermocapillary system.

A. Actuation principle

A detailed explanation of the use of thermocapillary convective flow for non-contact actuation can be found in [27]. This subsection emphasizes the relevant characteristics of the flow and its effects on the particle movement.

Figure 1 shows a schematic representation of the actuation principle. A container filled with water is initially at state of repose (the fluid velocity is null) and at ambient temperature (293 K) at time t = 0 s. Then, a collimated laser beam coming from the top reaches the surface of the water at point $\mathbf{X}_{\text{las}}$. Part of this energy is absorbed by the liquid, converted into heat and then, propagated in the fluid. The generated temperature field in the fluid is symmetrical around the laser spot (Z-axis). The temperature gradient at the interface generates a surface tension stress profile that is compensated by a viscous stress. This onsets the flow motion across the entire fluid. Because the temperature gradient is symmetrical around the laser spot, the flow velocity is also symmetrical. The flow velocity depends on the considered position and time. The resulting flow velocity is the fastest nearby the laser spot where the temperature gradient is the largest and it is slower farther away from the laser spot where the temperature gradient is smaller [27].

A particle lying close enough to the laser spot is affected by the thermocapillary convective flow and it moves along the flow direction. This flow is axi-symmetrical around the laser spot axis, so it is easier to analyze the particle velocity $\dot{\mathbf{X}}_{\text{part}}$ on its polar coordinates: magnitude $\dot{r}_{\text{part}}$ and direction θ_{part} (see Fig. 3). These two values will depend on the relative position between the particle $\mathbf{X}_{\text{part}}$ and the laser $\mathbf{X}_{\text{las}}$ which is given by the laser-particle vector $\mathbf{X}_{\text{las-part}} = \mathbf{X}_{\text{part}} - \mathbf{X}_{\text{las}}$.

B. Thermocapillary system model proposal

Based on the qualitative description of the thermocapillary system provided in the previous section, a model of the thermocapillary system is proposed in fig. 4. It is assumed that the control of the magnitude of the velocity of the particle and the direction of the motion can be decoupled. Thus two models are defined. The "VelMag model" defines the magnitude of the velocity of the particle $\dot{r}_{\text{part}}$ in function of the distance between the laser and the particle $r_{\text{las-part}}$. The "Vel Direction model" defines the relation between the direction of the displacement θ_{part} and the relative orientation between the particle and the laser $\theta_{\text{las-part}}$.

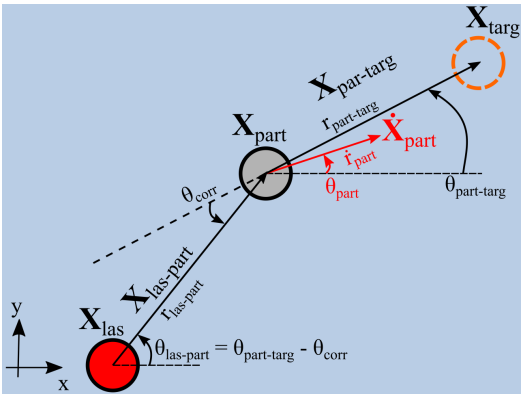

Fig. 3. Schematic representation of the variables involved in the system. At a given time instant, a particle at position $\mathbf{X}_{\text{part}}$ is displaced at velocity $\dot{\mathbf{X}}_{\text{part}}$, with magnitude $\dot{r}_{\text{part}}$ and direction θ_{part} towards a desired target location $\mathbf{X}_{\text{targ}}$. The particle velocity depends on the relative position between the particle and the laser spot $\mathbf{X}_{\text{las}}$, given by the vector $\mathbf{X}_{\text{las-part}}$ with polar coordinates: $r_{\text{las-part}}$ and $\theta_{\text{las-part}}$. Two controllers control these two components in real time so the particle reaches the target location $\mathbf{X}_{\text{targ}}$. The first controller allows to define $r_{\text{las-part}}$ in function of the magnitude of the particle-target vector $\mathbf{X}_{\text{part-targ}}$: $r_{\text{part-targ}}$. The second one defines a correction angle θ_{corr} that allows to deviate the particle velocity direction θ_{part} so that it tends to the desired direction which is the orientation of the particle-target vector $\mathbf{X}_{\text{part-targ}}$: $\theta_{\text{part-targ}}$. The presented sketch did not consider any scaling.

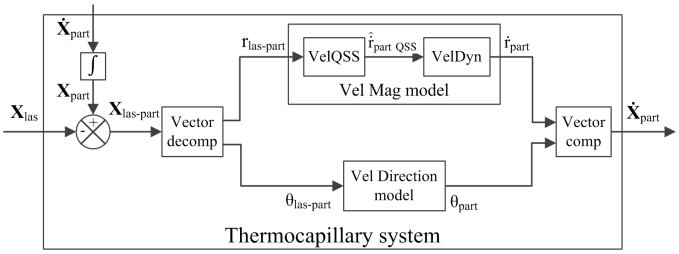

Fig. 4. Block diagram representation of the model proposed for the Thermocapillary system. The "Vel Mag model" block defines the relation between the particle velocity magnitude $\dot{r}_{\text{part}}$ and the laser-particle distance $r_{\text{las-part}}$. The "Vel Direction model" block defines the relation between the particle movement direction θ_{part} and the relative orientation between the particle and the laser spot $\theta_{\text{las-part}}$.

The conversion from cartesian coordinates (x, y) to polar coordinates (r, θ) and vice-versa is made in the "Vector decomp" and "Vector comp" blocks, respectively using standard relations. The particle position $\mathbf{X}_{\text{part}}$ is obtained by integrating the particle velocity $\dot{\mathbf{X}}_{\text{part}}$.

C. Methodology of the experimental identification

The "Vel Mag model" block (fig. 4) is identified based on its step response to a given laser-particle distance $r_{\text{las-part}}$. In order to do so, a constant laser-particle distance $r_{\text{las-part}}$ is imposed at each time instant. To accomplish this, the particle position $\mathbf{X}_{\text{part}}$ is measured using visual feedback and then, it is used to compute and define a new laser position $\mathbf{X}_{\text{las}}$ constantly.

The "Vel Direction model" block (fig. 4) is also identified experimentally also based on the step response of the block to a given laser-particle orientation $\theta_{\text{las-part}}$.

The models for the particle velocity magnitude $\dot{r}_{\text{part}}$ and direction θ_{part} are assumed to be independent. Therefore, it is possible to set a given laser-particle distance $r_{\text{las-part}}$ and a given laser-particle orientation $\theta_{\text{las-part}}$ and analyze their step responses independently.

Five laser-particle distances are tested: $r_{\text{las-part}}$ = 1.1, 1.5, 1.75, 2.0, 2.25 mm. On each test, the laser is placed at one of the four different orientations with respect to the particle: at the right, at the bottom, at the left and at the top ($\theta_{\text{las-part}}$ = 0°, 90°, 180°, 270°).

The methodology for the identification process for one given water sample is the following:

- A fresh distilled water sample is put into the container and then the 500-µm-diameter steel spherical particle is deposed at the water/air interface. The container is covered with a lid.
- One of the five laser-particle distances $r_{\text{las-part}}$ is chosen.
- For the chosen $r_{\text{las-part}}$, the laser is kept that distance away from the particle for at least 2 seconds with a given direction $\theta_{\text{las-part}}$. This test is carried on eight times, that is to say two times per orientation $\theta_{\text{las-part}}$. This same procedure is carried on for each of the 5 selected laser-particle distances $r_{\text{las-part}}$.
- Once all the distances have been tested, the particle and the container are cleaned using an ethanol solution.

This entire procedure was performed on 4 different water samples. Only one entire round of experiments is performed with each water sample because even using the lid, the surface keeps getting contaminated by surfactants that change the behavior of the thermocapillary convective flow [32].

D. Particle velocity magnitude model identification

The "Vel Mag model" block (fig. 4) defines the relation between the particle velocity magnitude $\dot{r}_{\text{part}}$ and the laser-particle distance $r_{\text{las-part}}$. This model is identified based on the step response of this block.

The experimentally measured particle velocity magnitudes $\dot{r}_{\text{part}}$ as a function of time for different laser-particle distances $r_{\text{las-part}}$ are shown in figure 5(a). Regarding the response time, overall, the system attains a quasi-steady state after around 0.8 s. As expected, the particle attains faster velocities when it is closer to the laser spot than when it is farther away in the range between 1.9-5 mm/s at quasi-steady. The standard deviation at quasi steady-state is in the range of 0.6-1.1 mm/s. It can also be noticed that the particle is moving even before the laser is turned on at t = 0 s, with a velocity up to 0.8 mm/s. This is due to fluid movement caused by motion of the air above the liquid surface and slight temperature variations on the liquid surface e.g. cooling from evaporation [33]. For control purposes, this velocity will be referred as the "noise" level in the following sections.

From figure 5(a), it can be seen that the measured particle velocity magnitude $\dot{r}_{\text{part}}$ for each given laser-particle distance $r_{\text{las-part}}$ can be modeled as a second order system with over-damp. However, the relation between the attained particle velocity at quasi steady-state, that will be referred as $\dot{r}_{\text{part QSS}}$ and the laser-particle distance $r_{\text{las-part}}$ is nonlinear. Taking this nonlinearity into consideration, it is proposed to use an estimation of the particle velocity at quasi steady-state $\hat{\dot{r}}_{\text{part QSS}}$ as an intermediate variable to define two subsystems as shown

in figure 4. The first subsystem ("VelQSS" block) is nonlinear and defines $\hat{\dot{r}}_{\text{part QSS}}$ in function of the laser-particle distance $r_{\text{las-part}}$. The second subsystem ("VelDyn" block) is a linear system represented by a second order transfer function which is used to model the dynamics of the system. Mathematically, this is expressed as follows:

$$\dot{r}_{\text{part}} = \underbrace{\hat{\dot{r}}_{\text{part QSS}}(r_{\text{las-part}})}_{\text{VelQSS}} \cdot \underbrace{\frac{\dot{r}_{\text{part}}}{\hat{\dot{r}}_{\text{part QSS}}}}_{\text{VelDyn}} \tag{2}$$

First, the "VelQSS" block is identified based on the analysis of the particle velocity magnitude at quasi steady-state $\dot{r}_{\text{part QSS}}$ in function of the input, the laser-particle distance $r_{\text{las-part}}$. Fourteen experiments are performed for laser-particle distances comprised between 1.1 and 4.5 mm. The corresponding particle velocity magnitudes at quasi steady-state are used to define a model to compute an estimation of this velocity using a linear fit:

$$\hat{\dot{r}}_{\text{part QSS}} = -1.366\, r_{\text{las-part}} + 5.706 \tag{3}$$

where: $\hat{\dot{r}}_{\text{part QSS}}$ is expressed in [mm s^{-1}] and $r_{\text{las-part}}$ is expressed in [mm]. The coefficient of determination for this estimation is $R^2 = 0.897$. As highlighted in our previous work [28], this low coefficient of determination is because there is an important variability in the particle motion for a given input (the steady-state velocity varies up to 1.1 mm/s.

Second, the "VelDyn" block is identified based on the dynamics of the particle velocity magnitude $\dot{r}_{\text{part}}$ in function of the intermediate variable $\dot{r}_{\text{part QSS}}$, which is computed using equation (3). The dynamics of the system is modeled using a second order transfer function, which has the general form:

$$H(s) = \frac{K_{\text{DC}}\,\omega_n^2}{s^2 + 2\zeta\omega_n s + \omega_n^2} \tag{4}$$

where: ω_n is the undamped natural frequency, ζ is the damping ratio and K_{DC} is the DC gain of the system.

The coefficients ω_n, ζ and K_{DC} are obtained for each curve presented in figure 5(a) using prediction error minimization [28]. The coefficients ω_n, ζ and K_{DC} do not vary significantly. So it is considered that the mean value of each of them is a fair enough representation of the system dynamics'. Using these results, the "VelDyn" block is defined as:

$$\text{VelDyn}(s) \equiv \frac{\dot{r}_{\text{part}}}{\hat{\dot{r}}_{\text{part QSS}}} = \frac{63.66}{s^2 + 13.9s + 63.66} \tag{5}$$

where: $\dot{r}_{\text{part}}$ and $\hat{\dot{r}}_{\text{part QSS}}$ are expressed in [mm s^{-1}].

In order to validate the proposed model, in figure 5(a), the mean particle velocity magnitudes $\dot{r}_{\text{part}}$ for the laser-particle distances $r_{\text{las-part}}$: 1.1, 1.5, 1.75, 2.0, 2.25 mm obtained from the experimental data are plotted in function of time, together with the curves obtained using the identified model. In terms of the particle velocity magnitude values, the difference between the predicted values and the real ones are expected because the model used to estimate the particle velocity magnitude at quasi steady-state $\hat{\dot{r}}_{\text{part QSS}}$ in function of $r_{\text{las-part}}$ had a correspondence value R^2 of 0.897. With this accuracy, the model could not be used to perform an accurate open-loop control of the system. However, its accuracy is fair enough for closed-loop control. The errors of the model are equivalent to perturbations and they will be rejected by the controller.

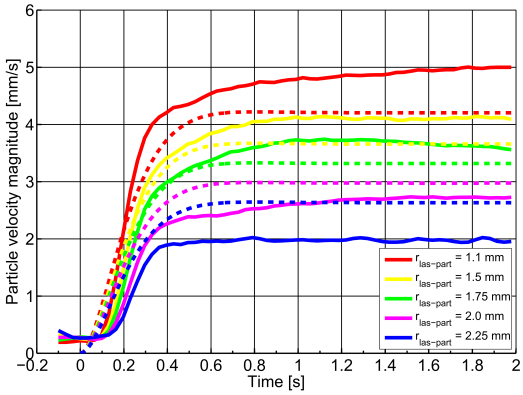

(a) Particle velocity magnitude $\dot{r}_{\text{part}}$. Comparison of characterized model against the experimental data. The solid lines correspond to the mean curve obtained from the experimental data for a given laser-particle distance. The dashed lines correspond to the curves obtained using the identified model.

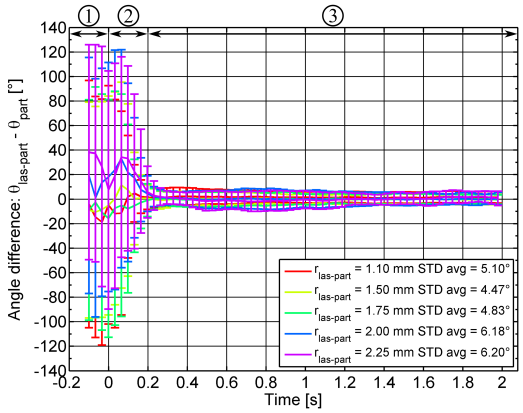

(b) Difference between the laser-particle orientation $\theta_{\text{las-part}}$ and the particle velocity direction θ_{part}. The plot represents the average angle difference among all the tests using the same laser-particle distance together with the error bar representing the standard deviation. In the legend, the average standard deviations (STD avg) at quasi steady-state (after 0.2 s) for each curve are shown.

Fig. 5. Particle velocity magnitude and direction in function of time, when the laser beam is pointed 1.1, 1.5, 1.75, 2.0, 2.25 mm away from a 500 µm spherical steel particle starting at time $t = 0$ s. The test rounds were performed in 4 different water samples. These trials were performed shortly after the distilled water was deposed on the container.

E. Particle velocity direction model identification

The "Vel Direction model" block (fig. 4) defines the relation between the particle velocity direction θ_{part} and the laser-particle orientation $\theta_{\text{las-part}}$. To identify it, the step response of the model is analyzed. As said in section III-C, the laser spot was positioned at different angles with respect to the position of the particle ($\theta_{\text{las-part}} = 0°, 90°, 180°, 270°$). The resulting particle velocity direction θ_{part} for each test was measured.

The difference between the laser-particle orientation $\theta_{\text{las-part}}$ and the particle velocity direction θ_{part} for every test is computed and shown in figure 5(b). To facilitate the analysis, the temporal evolution of the angle difference is divided in 3

phases. Phase 1 considers the time before the actuation begins at $t = 0$ s, where the angle difference is significant because, as mentioned in section III-D, the particle has an initial velocity and movement direction even before the laser is turned on. On phase 2, it can be seen that the angle difference decreases with time as the flow onsets, and after around 0.2 s, the angle difference attains a quasi steady-state close to 0°, which means that $\theta_{\text{part}} = \theta_{\text{las-part}}$. On phase 3, the angle difference remains at quasi steady-state with some small oscillations. The standard deviation at quasi steady-state is in the range of 4.4-6.2°. Overall, it can be noticed that the laser-particle distance $r_{\text{las-part}}$ does not have any effect in the variability of the results, neither in the settling time which remains around 0.2 s for all the cases.

From these results, the transfer function between the laser-particle orientation $\theta_{\text{las-part}}$ and the particle velocity direction θ_{part} can be considered to be identity. The value of $\theta_{\text{las-part}}$ converges to the value of θ_{part} in around 0.2 s. This settling time is 4 times faster than the settling time of the particle velocity magnitude $\dot{r}_{\text{part}}$ which was 0.8 s. Because of this, the dynamics of this subsystem is neglected. The small oscillations in the quasi steady-state response are considered to be almost negligible. However, a controller will be used to compensate the inaccuracy of the model.

IV. Controllers design

The goal of the controllers is to displace the particle from a given position $\mathbf{X}_{\text{part}}$ to a target position $\mathbf{X}_{\text{targ}}$. The control principle is presented in section IV-A, based on the models developed in section III. A PD controller is defined to control the particle velocity magnitude $\dot{r}_{\text{part}}$ in section IV-B and a P controller is defined to control the particle velocity orientation θ_{part} in section IV-C. Section IV-D deals with the choice of the gain values for the controllers.

A. Control principle

Since the transfer function of the Controlled mirror system is equal to identity (see section II-B), only the control of the thermocapillary system is discussed here (fig. 6 right part).

The goal of this section is to define the architecture of a closed-loop control scheme to control the particle velocity $\dot{\mathbf{X}}_{\text{part}}$. Inversion-based control is performed, based on the models of the thermocapillary system defined in the previous sections. As mentioned above, the particle velocity magnitude and its direction of motion can be decoupled. Thus two single-input single-output (SISO) systems are defined.

The first SISO system controls the particle velocity magnitude $\dot{r}_{\text{part}}$ and has as input the intermediate variable $\hat{\dot{r}}_{\text{part QSS}}$ (estimated particle velocity magnitude at quasi steady-state). This choice was made because $\hat{\dot{r}}_{\text{part QSS}}$ has a linear relation with $\dot{r}_{\text{part}}$ (see section III-D).

The second SISO system controls the particle velocity direction θ_{part} and has as input a correction angle θ_{corr}.

The control of the particle velocity consists thus in controlling two independent linearized systems: one relating $\hat{\dot{r}}_{\text{part QSS}}$ and the particle velocity magnitude $\dot{r}_{\text{part}}$, and the second one relating θ_{corr} and θ_{part}. To do so, a desired laser position $\mathbf{X}_{\text{lasD}}$ must be computed based on the inversion of the models defined in the previous sections, as follows.

The radial component of vector $\mathbf{X}_{\text{las-part}}$: $r_{\text{las-part}}$ is computed based on the resulting estimated particle velocity at quasi steady-state $\hat{\dot{r}}_{\text{part QSS}}$. This relation is obtained from the inversion of the model given by equation (3) (section III-D). This inverted model defines the laser-particle distance $r_{\text{las-part}}$ in function of $\hat{\dot{r}}_{\text{part QSS}}$ ("Vel Mag Inv equation" block) as:

$$r_{\text{las-part}} = -0.732\,\hat{\dot{r}}_{\text{part QSS}} + 4.177 \tag{6}$$

where: $r_{\text{las-part}}$ is expressed in [mm] and $\hat{\dot{r}}_{\text{part QSS}}$ in [mm s^{-1}].

The orientation of the laser-particle vector $\mathbf{X}_{\text{las-part}}$: $\theta_{\text{las-part}}$ is computed based on the correction angle θ_{corr}. This relation is applied into the system on the "Las-part Orient adjust equation" block and is given by the following equation:

$$\theta_{\text{las-part}} = \theta_{\text{part-targ}} - \theta_{\text{corr}} \tag{7}$$

where $\theta_{\text{part-targ}}$ is the desired orientation, the orientation of the particle-target vector $\mathbf{X}_{\text{part-targ}}$. The three variables are expressed in [°]. The detailed explanation of how θ_{corr} is used to adjust the particle movement direction is presented in section IV-C.

From the laser-particle distance $r_{\text{las-part}}$ and laser-particle orientation $\theta_{\text{las-part}}$, the laser-particle relative position $\mathbf{X}_{\text{las-part}}$ is computed in the "Vector Comp" block. The corresponding desired laser position $\mathbf{X}_{\text{lasD}} = \mathbf{X}_{\text{part}} - \mathbf{X}_{\text{las-part}}$ is then computed.

The next sections deal with the choice of the controllers for each of these two subsystems.

B. Particle velocity magnitude controller

The particle velocity magnitude controller (fig. 6 upper left part) controls the first SISO system which has as input the estimated particle velocity magnitude at quasi steady-state $\hat{\dot{r}}_{\text{part QSS}}$ and as output the particle velocity magnitude $\dot{r}_{\text{part}}$. The goal of this controller is to reduce the difference in distance between the target position $\mathbf{X}_{\text{targ}}$ and the particle position $\mathbf{X}_{\text{part}}$. In other words, the goal is to reduce the magnitude of the particle-target vector $\mathbf{X}_{\text{part-targ}} = \mathbf{X}_{\text{targ}} - \mathbf{X}_{\text{part}}$. So, the error for the particle velocity magnitude controller r_{error} is equal to the radial component of the particle-target vector $r_{\text{part-targ}}$. This error ($r_{\text{error}} = r_{\text{part-targ}}$) is used to compute the PD controller response, which in this case corresponds to the estimated particle velocity magnitude at quasi-steady state $\hat{\dot{r}}_{\text{part QSS}}$ ("Control Vel Mag" block).

For this controller, it is considered that the target position $\mathbf{X}_{\text{targ}}$ is reached when the particle enters a tolerance region defined as a circle with radius 250 µm around the target position $\mathbf{X}_{\text{targ}}$. As the infrared laser cannot be turned-off during operation, it was chosen to place the laser at the bottom edge of the working space when actuation stops. If the particle gets out of the tolerance region ($r_{\text{error}} \geq 250\,\mu\text{m}$), the actuation would restart.

C. Particle velocity direction controller

The particle velocity direction controller (fig. 6 bottom left part) controls the second SISO system which has as input the

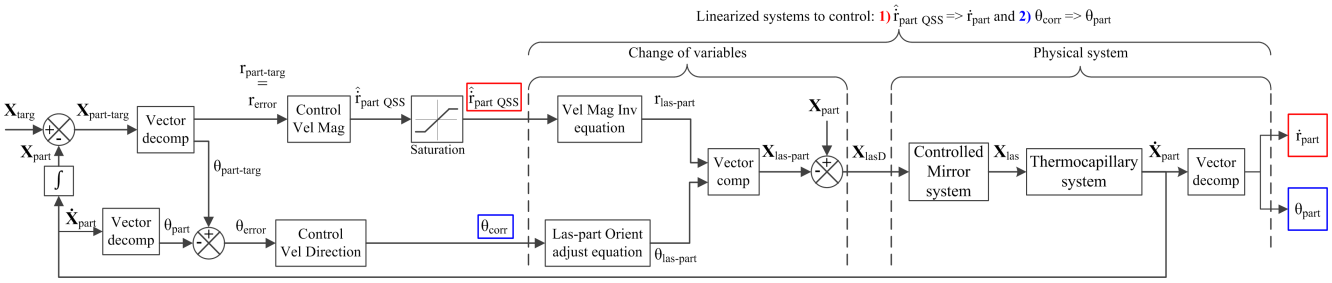

Fig. 6. Block diagram representation of the entire closed-loop system. The linearization of the physical system (Mirror and Thermocapillary systems) defines two subsystems which are shown at the right part of the figure. The first one has as input the estimated particle velocity magnitude at quasi steady-state $\hat{\dot{r}}_{\text{part QSS}}$ and as output the particle velocity magnitude $\dot{r}_{\text{part}}$ (enclosed in red). The second one has as as input the correction angle θ_{corr} and has as output the particle velocity direction θ_{part} (enclosed in blue). The first one is controlled by the particle velocity magnitude controller (upper left part) and the second one by the particle velocity direction controller (bottom left part).

correction angle θ_{corr} and has as output the particle velocity direction θ_{part}, as shown in the global control scheme. The goal of the direction controller is to reduce the difference between the particle velocity direction θ_{part} and the desired movement direction, which in this case is the orientation of the particle-target vector $\mathbf{X}_{\text{part-targ}}$: $\theta_{\text{part-targ}}$. So the error of the particle velocity direction controller θ_{error} is defined as follows:

$$\theta_{\text{error}} = \theta_{\text{part-targ}} - \theta_{\text{part}} \tag{8}$$

where the three variables are expressed in [°]. This value is used to compute the controller response, which in this case is the correction angle θ_{corr}, using a P control law ("Control Vel Direction" block).

As shown in figure 3, the correction angle θ_{corr} allows to deviate the commanded direction: the laser-particle orientation $\theta_{\text{las-part}}$ from the desired direction: the particle-target orientation $\theta_{\text{part-targ}}$. In case the error would be zero ($\theta_{\text{error}} = 0°$): the laser, the particle and the target positions would be collinear ($\theta_{\text{las-part}} = \theta_{\text{part-targ}}$) and no correction would be required, thus $\theta_{\text{corr}} = 0°$. But if the particle velocity direction θ_{part} would be deviated from the desired direction $\theta_{\text{part-targ}}$ ($\theta_{\text{error}} \neq 0°$), the laser-particle orientation $\theta_{\text{las-part}}$ would be deviated by a value given by the correction angle $\theta_{\text{corr}} \neq 0°$ according to relation (7). By doing so, the error in direction θ_{error} would be reduced gradually as time passes.

During the first time instants of the controlled manipulations, the particle velocity is low and is close to the "noise" level of 0.8 mm/s. In consequence, the particle velocity direction θ_{part} is highly noisy at the beginning and becomes less noisy as the particle velocity increases above the noise level. Therefore, the particle velocity direction controller is deactivated for the first second of the controlled manipulation, which enables the particle to attain a reasonable velocity above the noise level.

Similar to the particle velocity magnitude controller, this controller is also turned off when the particle attains the tolerance region around the target position ($r_{\text{error}} < 250\,\mu\text{m}$) and is turned on again if the particle gets out of it.

D. Controllers specifications

In order to test the system, two arbitrary performance goals are established for the particle velocity magnitude controller. The first goal is to have a settling time of 2 s and an overshoot of 10%. The second goal is to have a settling time of 2 s and an overshoot of 1%. These goals define the gains for Controllers A and B, respectively. The controllers gains are computed based on the identified model in section III-D. To determine the values for the gains, a method based in the dominant poles assignment method is used [34]. The results show that the integral gain K_{i} is almost zero, so it was decided to only take the proportional and derivate gains (K_{p} and K_{d} respectively) which define a PD controller. For controller A, the gains are: K_{p}=3.09, K_{i}=1.67. For controller B: K_{p}=1.148, K_{i}=0.332.

Regarding the particle velocity direction controller, only a proportional controller is used. This because, as shown in section III-E, the correspondence between the laser-particle orientation $\theta_{\text{las-part}}$ and the attained particle velocity direction θ_{part} was close to identity. Therefore the control of the orientation is not considered critical and a proportional controller with a proportional gain of 0.5 is applied to the controlled variable, the correction angle: $\theta_{\text{corr}} = 0.5\,\theta_{\text{error}}$.

V. Experimental Tests

This section presents the experimental results obtained using the controllers proposed in the previous section.

A. Experimental results on the displacement phase

The goal is to displace the particle towards a target position $\mathbf{X}_{\text{targ}}$. In the scope of this paper, only the time interval on which the particle is taken from a given position $\mathbf{X}_{\text{part}}$ towards the tolerance region around the target position $\mathbf{X}_{\text{targ}}$ is considered. All the plots presented in this section, stop at the time when the particle reaches the tolerance region for the first time. The exception is figure 9 which shows the controller attempting to stabilize the particle position at $\mathbf{X}_{\text{part}}$.

The error in distance r_{error} (fig. 7(a)) confirms that the particle can be moved towards a given target position $\mathbf{X}_{\text{targ}}$. Regarding the performance, controller A achieved the goal faster than controller B. Specifically, the last part of the manipulation is particularly difficult for controller B. The explanation for this is that controller A computed, overall, smaller laser-particle distances $r_{\text{las-part}}$ than controller B (fig. 7(b)). This means that controller A imposes, overall, faster

particle velocities than controller B. This is corroborated in figure 8(a), which plots the particle velocity magnitude $\dot{r}_{\text{part}}$ as function of time. This is beneficial for the control because it prevents the controller from operating close to the "noise" level of 0.8 mm/s (see section III-D). As it was seen in figure 7(a), the control of the particle movement becomes difficult whenever the particle velocity drops around the "noise" level.

In addition to the mentioned position error, another parameter to analyze is the motion accuracy. To do so, it is considered that the ideal/optimal trajectory is a line connecting the particle initial position and the target position. Taking this trajectory as a reference, the maximum error in distance would be of 0.67 mm and the average error STD would be 0.09 mm.

Another point to notice is the variability in the attained particle velocities. In the first time instants, the responses of both controllers are at saturation levels, however the resulting particle velocities on each experiment are different. Experiments 1 and 3 presented the fastest velocities for each controller with maximal velocities up to 9 mm/s and 7 mm/s respectively, while experiments 2 and 4 presented slower velocities up to 4.5 mm/s and 5 mm/s respectively. The main reason for this variability is the presence of different amounts of surfactants in each one of the samples. Such surfactants affect significantly the surface tension and thus the generated convective flow [32]. As a result, the attained flow velocity and, in consequence, the particle velocity are reduced. However, despite this variability, the target position is reached always.

Regarding the particle velocity direction controller, the error in direction θ_{error} as function of time is shown in figure 8(b). Considering the time instants between 1-3 s when the system operates at full velocity, the maximum error is a peak of 19.78° and the average error STD is 5.34° among all the experiments. However, as said before, as the system begins operating close to the "noise" level, the control over the particle becomes more difficult. For the movement direction, this means that the noise causes the particle to move on a random direction. A suitable controller would guarantee a large enough particle velocity even close to the tolerance region in order to have complete control over the particle movement. This is to be considered in future works.

Some pictures of the particle displacement performed in experiment 2 are shown in figure 10, where it can be seen how the particle is displaced towards the target position.

B. Discussion on the particle positioning problem

A delicate point to address is the problem of the particle position stabilization, which is not possible using the current control strategy. The two reasons for this are a "bouncing back effect" and the noise in the particle velocity. To illustrate these two effects, the particle trajectory in experiments 1 (Fig. 9a and 9b) and 3 (Fig. 9c and 9d) close to the target position is plotted.

In experiment 1 (Fig. 9a), the particle enters the tolerance region with a velocity of 4 mm/s (Fig. 8(a)) and then travels a distance of around 450 µm before stopping. However, after that the particle bounces back, exiting the tolerance region. Once this happens, the controllers are turned on again until

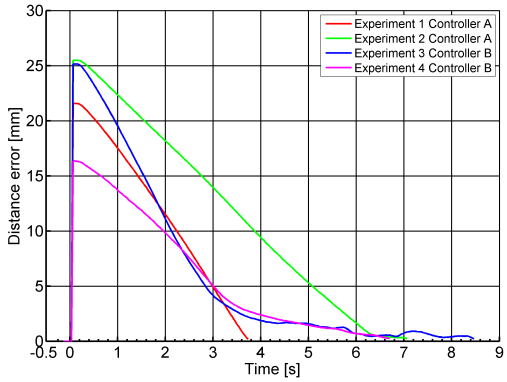

(a) Particle velocity magnitude controller error r_{error} in function of time.

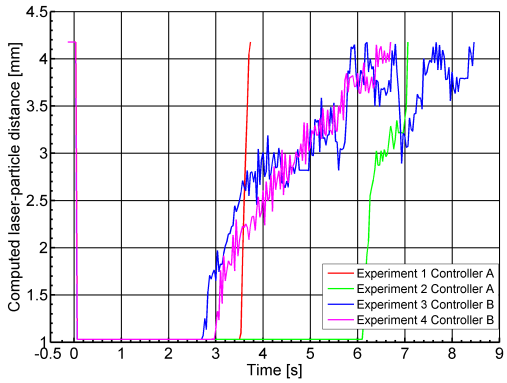

(b) Resulting laser-particle distance $r_{\text{las-part}}$ computed by the particle velocity magnitude controller in function of time.

Fig. 7. Relation between the input (r_{error}) and the computed response ($r_{\text{las-part}}$) of the particle velocity magnitude controller. At the beginning of the experiment, the particle is far from the target thus the laser is pointed close to the particle to reach high velocities. As the distance between the particle and the target decreases the laser is moved away from the particle.

the particle enters the tolerance region (Fig. 9b). However, again the particle travels a certain distance before bouncing back, exiting the tolerance region.

This "bouncing back effect" seems to occur due to a counter flow generated when the laser stops heating the region close to the particle. When this happens, some cold flow is still dragged to the surface due to fluid inertia. As the laser is not heating anymore, this fluid is colder than the fluid surrounding it. This generates a thermocapillary convective flow going inwards the position where the laser was which pulls the particle backwards. This phenomenon makes very difficult to stabilize the particle position using this control strategy as the particle would be constantly going in and out the tolerance region.

The second reason why controlling the particle final position is challenging comes from the difficulty to controls the particle motion at low velocities, close to the "noise" level. As it can be seen in Fig. 9c and 9d, the particle follows a chaotic trajectory before entering the tolerance region. Then, the "bouncing back" effect pulls it backwards. To avoid losing control over the particle velocity direction, the system needs to operate at velocities above the noise level. However, the consequence of this is that the particle cannot be smoothly placed at the target location. A specific control strategy that can stabilize

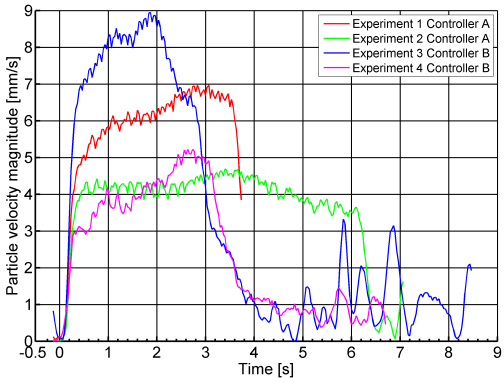

(a) Measured particle velocity magnitude $\dot{r}_{\text{part}}$ in function of time.

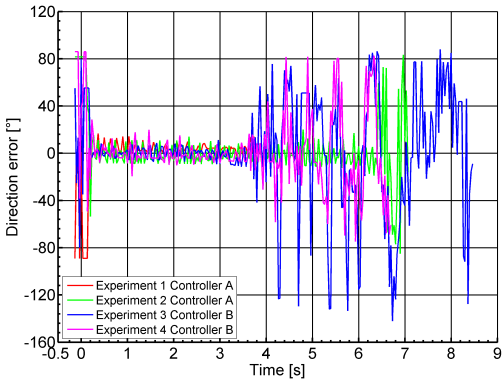

(b) Particle velocity direction controller error θ_{error} in function of time. The large error at the end when the particle is close to the target position $\mathbf{X}_{\text{targ}}$ occurs because the particle velocity magnitude $\dot{r}_{\text{part}}$ imposed in the particle is close to the "noise" level.

Fig. 8. Closed loop control of the particle velocity magnitude and direction.

the particle position will be proposed in the future.

C. Discussion on the performances of the proposed method

The results demonstrate that the thermocapillary convective flow can be used as an actuation principle for particle displacement. A 500-µm-diameter steel particle is displaced towards the target position with speeds between 4.5-9 mm/s which can be compared against some of the fastest manipulation techniques that use Marangoni effect. To mention some of them: glass particles with sizes up to 92 µm are manipulated at speeds up to 5.5 mm/s in [26], 20 µm diameter polystyrene particles are manipulated with speeds up to 200 µm/s in [23]. The proposed technique can manipulate particles more than 5 times bigger than the ones reported, heavier than the ones used in the reported experiments, with velocities in comparison to the fastest reported results.

In this article, steel spherical particles with a diameter of 500 µm are manipulated. However, one of the main advantages of this technique is that the particles will attain the flow velocity at steady-state regardless of their size. Small particles (below 50 µm) will attain the flow velocity almost instantly. Due to this property, there are used in Particle Tracking Velocimetry (PTV) to estimate the flow velocity of the entire fluid. The thermocapillary convective flow can also be used

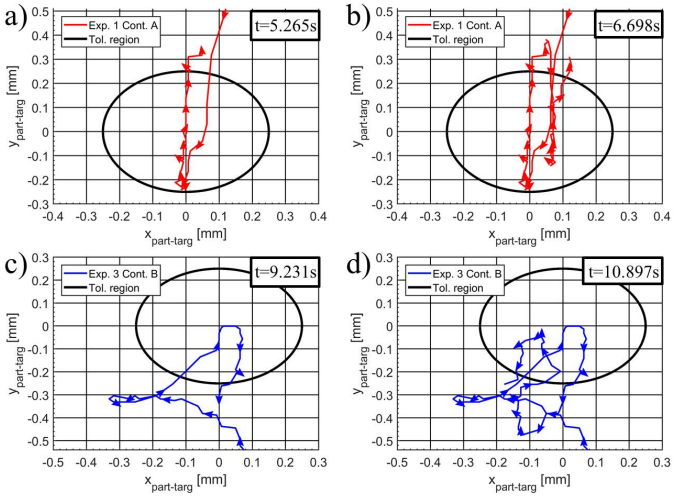

Fig. 9. Particle trajectory close to the target location. Figures a and b correspond to experiment 1 and figures c and d to experiment 3. The arrows represent only the particle velocity direction not its magnitude. The black circle represents the tolerance region.

for large particles, as long as they float and remain at the interface. If this will occur or not, will depend in the particle density and the particle/liquid contact angle. In our previous work [27], it was shown experimentally that particles with a diameter of 1000 µm can be manipulated using the proposed technique.

A comparison of the current technique against three techniques: magnetic manipulation, dielectrophoresis (DEP) and optical tweezers is presented in a recent work [28], which will be shortly discussed here. The manipulation using thermocapillary convective flows allows to manipulate objects in the entire micrometric scale 1-1000 µm whereas methods like the DEP and optical tweezers are limited to objects smaller than 100 µm. The attainable workspace can be large, in the order of several 10x10 mm^2, since it is determined by the deflection angle of the mirror and the liquid-mirror distance. The attainable force is large, in the order of tens of nN, and the attainable particle velocity is fast, in the order of few mm/s. These two results are comparable to the ones obtained with DEP but below the ones obtained with magnetic manipulation. Another drawback is that the system is naturally unstable due to repulsive force exerted in the particle. So in order to control the particle position, a controller is required which is the motivation in this paper to develop a closed-loop controller for the system.

In addition to these advantages and drawbacks, the proposed technique has two differentiating features. The first one is that the force is locally applied due to the localized nature of the generated flows, which is different from magnetic or DEP manipulation where the force is applied in the entire workspace. This opens the path for the manipulation of multiple particles in parallel. The second difference is the manipulability criterion, which is that the particles should float. This is determined by the particle density and its particle/liquid contact angle. This is different from the magnetic manipulation that can only be used on magnetic particles, the DEP that requires certain electric permittivity in the particle or the optical tweezers that

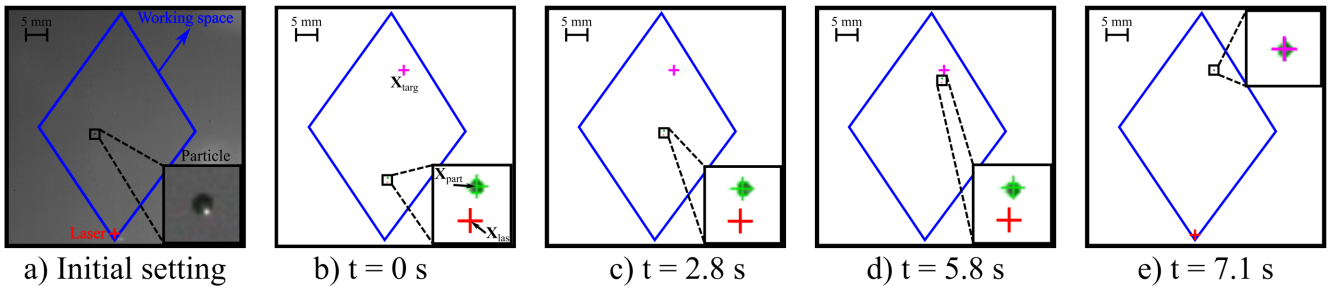

Fig. 10. Controlled manipulation corresponding to experiment 2 in section V-A. a) Initial setting: a 500-µm-diameter spherical steel particle is floating on the surface of a water layer with the particle velocity magnitude and direction controllers turned off, so the laser spot (red cross) is placed at the bottom part of the working space (blue rhombus). b) The backlight is turned on and then, at t = 0 s, both controllers are turned on. The particle is at position $\mathbf{X}_{part}$ (green cross) and the goal is to displace it to the target position $\mathbf{X}_{targ}$ (magenta cross) by changing the position of the laser spot $\mathbf{X}_{las}$ (red cross). c, d) The particle is displaced towards the target position. e) The particle reaches the tolerance region around the target position, so the two controllers are turned off. (*This experiment is shown in the video available as supplementary material*).

require a large refraction index. Due to these differentiating features, the proposed method can be seen as an attractive alternative to other methods, offering good performances in terms of velocity and force.

As mentioned above, the proposed technique allows to displace the particles in the plane defined at the water/air interface. The applicative interest of such planar manipulation is described in several papers [35–38]. The most promising application is linked with micro-factories, especially the transfer of small components between assembly workstations due to the large workspace of the proposed technique (several 10x10 mm^2). For objects that are not compatible with water (e.g. materials sensible to corrosion), other liquid media such as alcohol and oil could be used.

VI. Conclusions

In this work, a model for a non-contact actuation system based on laser-induced thermocapillary convective flows has been proposed and experimentally identified. The physical principle that onsets the flow motion and thus the movement of the objects placed at the air/water interface has been studied. From this study, it was shown there was a dependence of the particle velocity magnitude and direction on the relative position of particle with respect to the laser. This dependence is modeled and two controllers are proposed: a PD controller for the particle velocity magnitude and a P controller for the particle velocity direction.

Proof of concept experiments are performed on which a 500-µm-diameter steel spherical particle is displaced towards the vicinity of a target position. Maximal velocities up to 4-9 mm/s are attained during the control phase, which can be compared with the fastest manipulation techniques that use Marangoni effect.

A control strategy able to control the particle final position will be proposed in future works. It must cancel or compensate the noise and also counteract the particle bounce back. Complex light patterns might be used to create stable positions so that the particle can be stopped at a given location. The controller robustness will also be studied in more details by manipulating particles with different shapes and sizes and also performing trajectory tracking.

Acknoledgements

This research has been funded by the Interuniversity Attraction Poles Programme (IAP 7/38 MicroMAST) initiated by the Belgian Science Policy Office, by the Labex ACTION project (contract "ANR-11-LABX-01-01"), and by the Région Franche-Comté. This work has also been carried out in relation with the COST Action MP1106 on Smart and Green Interfaces. The authors thank Prof. Pascal Kockaert and Prof. Pierre Colinet for their valuable scientific advice.

References

[1] B. J. Nelson, I. K. Kaliakatsos, and J. J. Abbott, "Microrobots for minimally invasive medicine," *Annual review of biomedical engineering*, vol. 12, pp. 55–85, 2010.

[2] S. Bouchebout, A. Bolopion, J.-O. Abrahamians, and S. Régnier, "An overview of multiple dof magnetic actuated micro-robots," *Journal of Micro-Nano Mechatronics*, vol. 7, no. 4, pp. 97–113, 2012.

[3] I. S. Khalil, L. Abelmann, and S. Misra, "Magnetic-based motion control of paramagnetic microparticles with disturbance compensation," *IEEE Transactions on Magnetics*, vol. 50, no. 10, pp. 1–10, 2014.

[4] H. Marino, C. Bergeles, and B. J. Nelson, "Robust electromagnetic control of microrobots under force and localization uncertainties," *IEEE Transactions on Automation Science and Engineering*, vol. 11, no. 1, pp. 310–316, 2014.

[5] E. Diller, J. Giltinan, G. Z. Lum, Z. Ye, and M. Sitti, "Six-degree-of-freedom magnetic actuation for wireless microrobotics," *Int. J. Rob. Res.*, vol. 35, no. 1-3, pp. 114–128, Jan. 2016.

[6] F. Long, D. Matsuura, and C. H. Menq, "Actively controlled hexapole electromagnetic actuating system enabling 3-d force manipulation in aqueous solutions," *IEEE/ASME Transactions on Mechatronics*, vol. 21, no. 3, pp. 1540–1551, 2016.

[7] E. Diller, J. Giltinan, and M. Sitti, "Independent control of multiple magnetic microrobots in three dimensions," *The International Journal of Robotics Research*, vol. 32, no. 5, pp. 614–631, Apr. 2013.

[8] E Diller, M Sitti, *et al.*, "Three-dimensional programmable assembly by untethered magnetic robotic micro-grippers," *Advanced Functional Materials*, vol. 24, no. 28, pp. 4397–4404, 2014.

[9] K. Yu, J. Yi, and J. W. Shan, "Motion control, planning and manipulation of nanowires under electric-fields in fluid suspension," *IEEE Transactions on Automation Science and Engineering*, vol. 12, no. 1, pp. 37–49, 2015.

[10] Z. D. Harms, D. G. Haywood, A. R. Kneller, L. Selzer, A. Zlotnick, and S. C. Jacobson, "Single-particle electrophoresis in nanochannels," *Analytical Chemistry*, vol. 87, no. 1, pp. 699–705, 2015.

[11] J. Voldman, "Electrical forces for microscale cell manipulation," *Annu. Rev. Biomed. Eng.*, vol. 8, pp. 425–454, 2006.

[12] J. Čemažar, D. Miklavčič, and T. Kotnik, "Microfluidic devices for manipulation, modification and characterization of biological cells in electric fields–a review," *Electronic Components and Materials*, vol. 43, no. 3, pp. 143–161, 2013.

[13] M. Kharboutly and M. Gauthier, "High speed closed loop control of a dielectrophoresis-based system," in *2013 IEEE International Conference on Robotics and Automation (ICRA)*, 2013, pp. 1446–1451.

[14] J. Zemánek, J. Drs, and Z. Hurák, "Dielectrophoretic actuation strategy for micromanipulation along complex trajectories," in *2014 IEEE/ASME International Conference on Advanced Intelligent Mechatronics*, 2014, pp. 19–25.

[15] F. Arai, K. Yoshikawa, T. Sakami, and T. Fukuda, "Synchronized laser micromanipulation of multiple targets along each trajectory by single laser," *Applied Physics Letters*, vol. 85, no. 19, pp. 4301–4303, 2004.

[16] K. Onda and F. Arai, "Parallel teleoperation of holographic optical tweezers using multi-touch user interface," in *IEEE International Conference on Robotics and Automation*, May 2012, pp. 1069 –1074.

[17] H. Chen, C. Wang, X. Li, and D. Sun, "Transportation of multiple biological cells through saturation-controlled optical tweezers in crowded microenvironments," *IEEE/ASME Transactions on Mechatronics*, vol. 21, no. 2, pp. 888–899, 2016.

[18] M. A. Burns, C. H. Mastrangelo, T. S. Sammarco, F. P. Man, J. R. Webster, B. N. Johnsons, B Foerster, D Jones, Y Fields, A. R. Kaiser, and D. T Burke, "Microfabricated structures for integrated dna analysis," in *Proceedings of the National Academy of Sciences of the United States of America, 93(11)*, vol. 93, 1996, pp. 5556–5561.

[19] M. Tanyeri, M. Ranka, N. Sittipolkul, and C. M. Schroeder, "A microfluidic-based hydrodynamic trap: design and implementation," *Lab on a Chip*, vol. 11, pp. 1786–1794, 10 2011.

[20] M. D. Armani, S. V. Chaudhary, R. Probst, and B. Shapiro, "Using feedback control of microflows to independently steer multiple particles," *Journal of Microelectromechanical Systems*, vol. 15, no. 4, pp. 945–956, 2006.

[21] W. Hu, K. S. Ishii, and A. T. Ohta, "Micro-assembly using optically controlled bubble microrobots," *Applied Physics Letters*, vol. 99, no. 9, 094103, 2011.

[22] K. Ishii, W. Hu, and A. Ohta, "Cooperative micromanipulation using optically controlled bubble microrobots," in *2012 IEEE International Conference on Robotics and Automation (ICRA)*, 2012, pp. 3443–3448.

[23] W. Hu, Q. Fan, and A. T. Ohta, "An opto-thermocapillary cell micromanipulator," *Lab Chip*, vol. 13, no. 12, pp. 2285–2291, 2013.

[24] ——, "Interactive actuation of multiple opto-thermocapillary flow-addressed bubble microrobots," *Robotics and Biomimetics*, vol. 1, no. 1, pp. 1–6, 2014.

[25] M. A. Rahman, J. Cheng, Q. Fan, and A. T. Ohta, "Automated actuation of multiple bubble microrobots using computer-generated holograms," in *Proceedings of SPIE*, vol. 9494, 2015, pp. 1–7.

[26] E. Vela, "Non-contact microscale manipulation using laser-induced convection flows," PhD thesis, Universite Pierre et Marie Currie, 2010.

[27] R. Terrazas Mallea, A. Bolopion, J.-C. Beugnot, M. Gauthier, and P. Lambert, "Laser-induced thermocapillary convective flows: a new approach for non-contact actuation at microscale at the fluid/gas interface," *IEEE/ASME Transactions on Mechatronics*, vol. 22, no. 2, pp. 693–704, 2017.

[28] R. Terrazas Mallea, A. Bolopion, J.-C. Beugnot, P. Lambert, and M. Gauthier, "1d manipulation of a micrometer size particle actuated via thermocapillary convective flows," in *IEEE/RSJ International Conference on Intelligent Robots and Systems*, 2017.

[29] A. Rapacchietta and A. Neumann, "Force and free-energy analyses of small particles at fluid interfaces:ii. spheres," *Journal of Colloid and Interface Science*, vol. 59, no. 3, pp. 555 –567, 1977.

[30] Q. Gao and N. Olgac, "Bounds of imaginary spectra of lti systems in the domain of two of the multiple time delays," *Automatica*, vol. 72, no. C, pp. 235–241, Oct. 2016.

[31] ——, "Stability analysis for lti systems with multiple time delays using the bounds of its imaginary spectra," *Systems & Control Letters*, vol. 102, no. Supplement C, pp. 112 –118, 2017.

[32] J. Berg and A. Acrivos, "The effect of surface active agents on convection cells induced by surface tension," *Chemical Engineering Science*, vol. 20, no. 8, pp. 737 –745, 1965.

[33] J. P. Longtin, K. Hijikata, and K. Ogawa, "Laser-induced surface-tension-driven flows in liquids," *International Journal of Heat and Mass Transfer*, vol. 42, no. 1, pp. 85 –93, 1999.

[34] G. M. Malwatkar and L. M. Waghmare, "Design of controllers for higher-order-plus-delay-time processes: a practical solution," *International Journal of Computer Applications*, vol. 1, no. 21, pp. 33–38, 2010.

[35] J. M. K. Ng, M. J. Fuerstman, B. A. Grzybowski, H. A. Stone, and G. M. Whitesides, "Self-assembly of gears at a fluid/air interface," *Journal of the American Chemical Society*, vol. 125, no. 26, pp. 7948–7958, 2003, PMID: 12823016.

[36] S. Gupta, N. Singh, M. Sastry, R. Kakkar, and R. Pasricha, "Controlling the assembly of hydrophobized gold nanoparticles at the air-water interface by varying the interfacial tension," *Thin Solid Films*, vol. 519, no. 3, pp. 1072 –1077, 2010, Biomolecular Electronics and Organic Nanotechnology for Environmental Preservation.

[37] P. Rogers, I. Gralinski, C. Galtry, and A. Neild, "Selective particle and cell clustering at air-liquid interfaces within ultrasonic microfluidic systems," *Microfluidics and Nanofluidics*, vol. 14, no. 3-4, pp. 469–477, 2013.

[38] M. Dkhil, M. Kharboutly, A. Bolopion, S. Regnier, and M. Gauthier, "Closed-loop control of a magnetic particle at the air-liquid interface," *IEEE Transactions on Automation Science and Engineering*, vol. 14, no. 3, pp. 1387–1399, 2017.

Ronald Terrazas Mallea received his M. E. degree from the EMARO program (European Master in Advanced Robotics), where he studied at École centrale de Nantes, France and at Warsaw University of Technology, Poland. He is currently working towards the Ph.D. degree in engineering sciences and technology at the Université Libre de Bruxelles, Belgium and the Ph.D. degree in automatics at the Université de Franche-Comté, France in the framework of double degree program. His research interests are micromanipulation via actuated flows, surface tension effects, automatic control and vision based control.

Aude Bolopion received her Ph.D. degree in robotics in 2010 from the University of Pierre et Marie Curie, Paris, France.

She is currently a CNRS researcher at the FEMTO-ST Institute, Besancon, France. She has been a member of the Biomedical Micro Nano Robotics team since 2011. From 2007 and 2011 she was a member of the ISIR micromanipulation team. Her research interests are focused on teleoperation and haptic feedback at the nanoscale, and on non-contact micromanipulation.

Jean-Charles Beugnot received the M.Sc. degree and the Ph.D. degree in electronics studies from the Université de Franche-Comté, France, in 2004 and 2007, respectively.

He is currently full-time CNRS researcher in the Optics department at FEMTO-ST Institute (France). During his career he stayed at Swiss Federal Institute of Technology of Lausanne, Switzerland and at Polytechnic University of Valencia, Spain. His research interests are microstructured fibers and their applications for fiber optic sensors, nonlinear optics in fibers, processing of optical information and opto-acoustic interactions.

Pierre Lambert received his PhD degree in engineering sciences from the Université Libre de Bruxelles, Belgium in 2004.

He is currently Associate Professor at Université Libre de Bruxelles, in the field of micro-engineering and microfluidics. He is the coordinator of the Belgian thematic network on Microfluidics and Micromanipulation: Multiscale Applications of Surface Tension (www.micromast.be). He is author or co-author of 32 journal papers and 39 conference papers. His current research interests are in the fields of soft robotics (tunable stiffness mechanisms, smart catheters) and of surface tension effects in microsystems (capillary gripping, capillary self-alignment, thermocapillary micromanipulation).

Michaël Gauthier received his PhD degree in Automation and Robotics from the Université de Franche Comté, France in 2002.

He is currently CNRS Senior scientist research at FEMTO-ST institute and the vice-head of FEMTO-ST. He has been granted by the French CNRS bronze medal (Early Career Award) in 2011. He is author or co-author of 28 journal papers and 42 conference papers in the field of micro-nano-robotics. His research interests are focused on microworld modeling, micro and nano manipulation, dexterous microhandling and high speed control of non-contact micromanipulations.